EXPLOSIVE PHASE TRANSITION IN LH_2

Vaagsaether, K.[1], Hansen, P.M.[1] and Bjerketvedt, D.[1]
[1] Dept. of Process, Energy and Environmental Technology, University of South-Eastern Norway, Kjolnes Ring 56, Porsgrunn, 3918, Norway, knutv@usn.no

ABSTRACT

This paper describes two models for analysing and simulating the physical effects of explosive phase transition of liquid hydrogen (LH_2), also known as cold BLEVE. The present work is based on theoretical and experimental work for liquefied CO_2. A Rankine Hugoniot analysis for evaporation waves that was previously developed for CO_2 is now extended to LH_2. A CFD-method for simulating two-phase flow with mass transfer between the phases is presented and compared with the Rankine Hugoniot analysis results. The Rankine Hugoniot method uses real fluid equations of state suited for LH_2 while the CFD method uses linear equations of state suited for shock capturing methods. The results show that there will be a blast from a catastrophic rupture of an LH_2 vessel and that the blast waves will experience a slow decay due to the large positive pressure phase.

1.0 INTRODUCTION

The construction of the necessary infrastructure requires knowledge-based risk assessments to ensure a safe operation of the process facilities. The rupture of a vessel, storage tank, or pipeline containing a pressurized liquefied gas held at a temperature above its atmospheric pressure boiling point constitutes a hazard that should be included in safety assessments. If the rupture and resulting release take place nearly instantaneously, the explosion can, under certain conditions be referred to as a boiling liquid expanding vapor explosion (BLEVE). Liquid hydrogen (LH_2) has saturation pressure at atmospheric pressure at about 20K. At higher temperatures, a tank containing saturated LH_2 will have higher pressures than the atmosphere. Heat added to an LH_2 tank will cause the pressure to increase along the saturation curve, as shown in Fig. 1, where the LH_2 is heated from 20.4 K to 29 K. An isentropic expansion will lead the hydrogen state into the two-phase region, causing phase transition. During a catastrophic failure of a tank, the expansion of the containing LH_2 can lead to large rates of gas-phase production. The rapid fluid expansion pushes the surrounding air and can cause pressure loads similar to gas explosions. Another possible scenario from heating LH_2 is for “full” tanks, where the liquid volume is initially 85% of the total tank volume. During possible heating of the LH_2, as shown in Fig. 2, the liquid expansion will lead to 100 % liquid volume in the tank. Further heating leads to constant volume pressure increase that will rapidly increase pressure.

Previous work on BLEVEs in CO_2 by Hansen et al. [1] is extended to LH_2 BLEVEs in this paper. The Rankine Hugoniot analysis and experimental work presented in [2] for CO2 are used to predict the behavior of LH_2 during rapid depressurization. The initial pressures will be lower for LH_2 than for CO_2, but a BLEVE is still possible from a vessel's catastrophic failure.

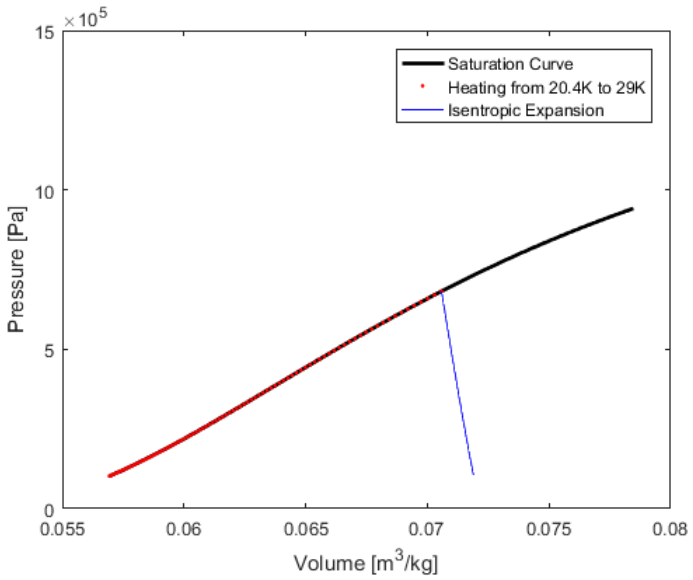

Figure 1: Thermodynamic process of heating saturated LH_2 from 20.4 K to 29 K followed by an isentropic expansion to atmospheric pressure.

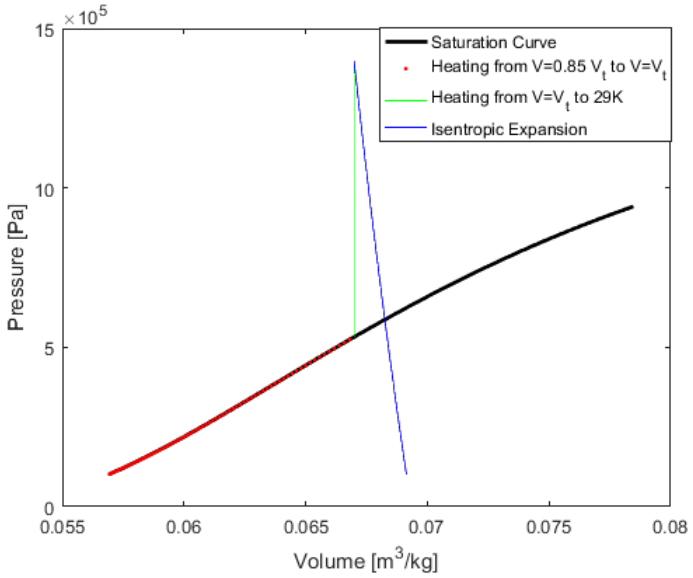

Figure 2: Example of processes during heating of LH_2 in the tank at 85% filling. The initial state is saturated LH_2 at 1 bara (20 K).

In the example described in figure 2, the liquid expands inside the tank up to a temperature of about 27.6 K. At this state, the liquid volume is the same as the tank volume. Further heating increases pressure at constant volume leading to a rapid pressure increase up to 29 K. The example assumes that the tank ruptures at 29 K, followed by an isentropic expansion of the liquid into the metastable region.

2.0 CALCULATION METHODS

The thermodynamic states are calculated by using an equation of state (EOS) based on Helmholtz free energy [3] and [4]. The maximum liquid expansion before phase transition can be approximated using the Nucleation Theory described in Blander and Katz [5].The rate of creation of number of bubbles pr. volume is calculated as equation 1.

$$dJ = J_0 \exp(-\frac{W_{cr}}{kT_0}), \quad (1)$$

The critical work is here simplified to eq. 2 by assuming the Poynting factor to be unity.

$$W_{cr} = \frac{16\pi\sigma^3}{3(p_{sat}(T)-p(T))^2}, \quad (2)$$

Where J_0 – initial possible nucleation sites, k – Boltzmann constant, T_0 – critical temperature, σ – liquid/gas surface tension.

2.1 Computational Fluid Dynamics

A two-fluid model for CFD simulations of the process uses mass, momentum, and energy conservation of two immiscible fluids (liquid and gas phases). The assumption here is that the momentum of each phase is given by a common velocity, leading to a five-equation model in 1D, or a seven equation model in 3D. Equations 3 and 4 are equations for mass conservation of the two phases, equation 5 is the equation for the common momentum, equations 6 and 7 are the energy equations for each phase.

$$\frac{\partial \rho_1 \alpha_1}{\partial t} + \nabla \cdot (\rho_1 \alpha_1 \vec{u}) = -\dot{R}, \quad (3)$$

$$\frac{\partial \rho_2 \alpha_2}{\partial t} + \nabla \cdot (\rho_2 \alpha_2 \vec{u}) = \dot{R}, \quad (4)$$

$$\frac{\partial \rho u}{\partial t} + \nabla \cdot (\rho \vec{u} u) + \frac{\partial p}{\partial x} = 0, \quad (5)$$

$$\frac{\partial \alpha_1 E_1}{\partial t} + \nabla \cdot (\alpha_1 \vec{u}(E_1 + p)) = -\dot{R} Q_{\mathrm{vap}}, \quad (6)$$

$$\frac{\partial \alpha_2 E_2}{\partial t} + \nabla \cdot \left(\alpha_2 \vec{u}(E_2 + p)\right) = \dot{R} Q_{vap}, \quad (7)$$

Where α_1 is the volume fraction of liquid and α_2 is the volume fraction of the gas. The volume fractions are related as $\alpha_1 + \alpha_2 = 1$ and $\rho_1 \alpha_1 + \rho_2 \alpha_2 = \rho$. The energies of each phase are calculated as equation 8.

And, p – pressure, u – fluid velocity, ρ – fluid density, Q_{vap} – heat of evaporation.

$$E_i = e_i + \frac{1}{2}\rho_i |\vec{u}|^2, \quad (8)$$

For the liquid phase, a stiffened gas equation of state is used to model the dependence of internal energy to pressure (see equation 9).

$$e_1 = \frac{p+\gamma_1 p_\infty}{\gamma_1 - 1}, \quad (9)$$

Ideal gas law is used for the gas phase (phase 2), equation 10.

$$e_2 = \frac{p}{\gamma_2 - 1} + e^*, \quad (10)$$

The constant e* is an energy term to set the correct difference in internal energy between the gas and liquid phase. Since the modeled internal energy is based on changes in internal energy, this term must be added to model the correct change of energy between the phases. The Flux Limiter Centered Scheme (FLIC) is used for solving the hyperbolic parts of the equation set, while a Newton-Rhapson iterative solver is needed to isolate volume fraction and pressure from the conserved mass and energies.

The phase transition mass rate, $\dot{R}$ in equation 11, is modeled using the nucleation rate in eq. 1.

$$\dot{R} = \rho_{g,sat}(T) V_{cr} dJ, \tag{11}$$

Where V_{cr} is the volume of a critical bubble and ρ_{sat} is the gas density of the critical bubbles. The radius of a critical bubble is calculated as equation 12.

$$r_{cr} = \frac{2\sigma}{p_{sat}(T) - p}, \tag{12}$$

The mass and energy sources are solved using Godunov splitting so that the hyperbolic part is solved using the FLIC scheme, and the sources are solved by a simple first-order Euler method.

Simulation set-up

Fig. 3 shows the initial simulation set-up in a quasi 1D, spherical coordinate system. The liquid phase is LH_2, and the initial gas phase is atmospheric air. Since air and gaseous hydrogen are assumed to have the same γ, the same energy term for the gas phase will be used for both gasses. The length of the liquid condition is 200 control volumes, and the total domain is 25 liquid radii (e.g. 5000 control volumes). Fig. 4 shows the initial values for pressure and liquid volume fraction. Table 1 shows the parameters used for the simulations of expansion from 9 bara saturated state.

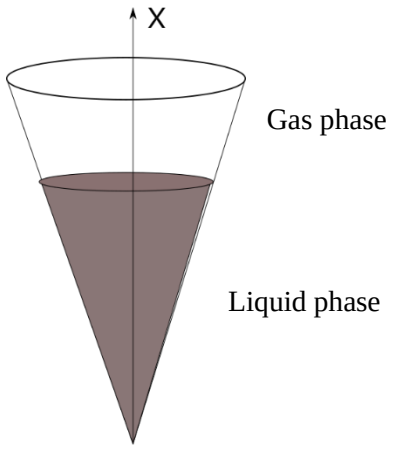

Figure 3: Simulation domain for two-fluid model.

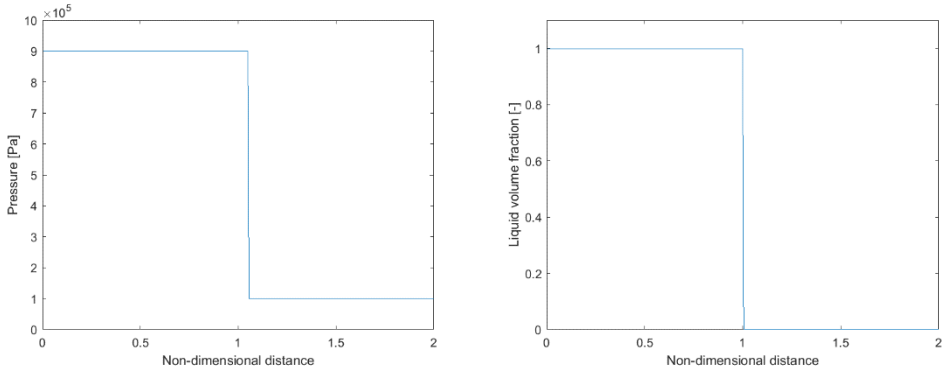

Figure 4: Initial pressure (Left) and liquid volume fraction (right) for 9 bara saturated liquid hydrogen expansion simulation.

Table 1: Parameter values used in the simulations for expansion from 9 bara.

Variable	Value
γ_1	1.4
γ_2	1.4
p_∞	$1.5 \cdot 10^7$ Pa
e*	$9 \cdot 10^5$ J/kg
σ	$3.1 \cdot 10^{-4}$ N/m
Q_{vap}	20 000 J/kg

2.2 Rankine Hugoniot relations

The propagation of adiabatic evaporation waves was modeled by the Rankine- Hugoniot relations that treated the wave as a jump between a superheated liquid state and a 2-phase equilibrium state. This subchapter describes the calculation method that was used in the current work. The method incorporates the ideas previously discussed by [6-17]. The analysis defines three states. A rarefaction wave (or fan) and an evaporation wave separate the states. Figure 5 illustrates the defined states, waves, and the control volume. State 0 (saturated liquid) is the initial pre-rupture state, located in front of the rarefaction wave. State 1 (superheated liquid) is the metastable liquid state, located behind the rarefaction wave but ahead of the evaporation wave. State 2 (two-phase equilibrium mixture) is located behind the evaporation wave. T is the temperature, P is the pressure, V is the specific volume, h is the enthalpy, u is the velocity, and χ is the vapor mass fraction. A control volume that includes state 1 and state 2 is drawn around the evaporation wave. The evaporation wave is restricted to a narrow region [11]. The enthalpy used to evaporate a fraction of the liquid originates from the rapid depressurization from the saturated liquid state to the superheated state.

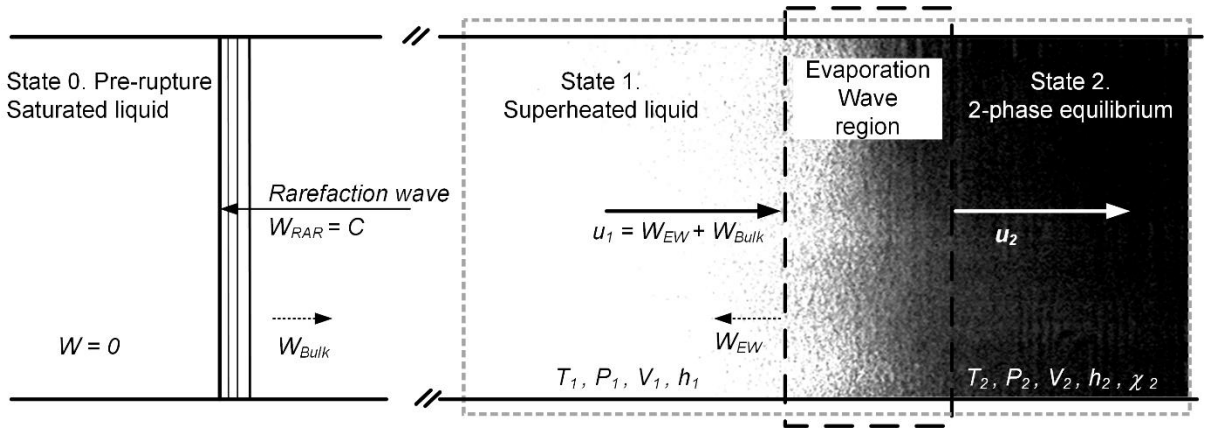

Figure 5: Control volume for Rankine Hugoniot analysis of the phase transition process during a BLEVE from liquefied gas.

Equation 13 is the combined mass and momentum conservation referred to as the Rayleigh line.

$$p_2 = -\left(\frac{u_1}{V_1}\right)^2 V_2 + \left(p_1 + \frac{u_1^2}{V_1}\right), \tag{13}$$

Equation 14 is the energy and momentum equation referred to as Hugoniot-curve. Equation 15 is the mass fraction of gas behind the phase transition front. Previous work [2] showed that the solution for the state behind the phase transition front is given at the tangent of the Rayleigh line at the Hugoniot curve, also called the Chapman-Jouget solution (CJ).

$$h_2 - h_1 = \frac{1}{2}(p_2 - p_1)(V_2 + V_1), \tag{14}$$

$$\chi_2 = \frac{2(h_1 - h_{l,2}) + (V_1 + V_{l,2})(p_2 - p_1)}{2(h_{v,2} - h_{l,2}) - (V_{v,2} - V_{l,2})(p_2 - p_1)}, \tag{15}$$

3.0 RESULTS

The Rankine Hugoniot analysis of expansion from saturated LH_2 at 6 bara and 9 bara is shown in Fig. 6. For the calculations, the liquid state is saturated at these conditions. The initial states are chosen to be far enough away from the critical point at about 13 bara. The initial states are also chosen as possible states along an isentrope where the expansion crosses the satuation curve. If the liquid is sub-cooled, the liquid expansion is thought to not contribute to the blast. This is an assumption that need more research since the total enthalpy in the fluid will be higher, e.g. it has kinetic energy at the saturated state. The failure pressure of tank is not known, but possible catastrophic failure of a tank contining sub-cooled LH_2 will pass the saturation curve on the liquid side. If the hydrogen is super critical the expansion will be different. The maximum expansion allowed in the calculation is for the isentropic expansion to either the kinetic spinodal or the thermodynamic spinodal. The kinetic spinodal is determined from equation 1, where the production rate of critical bubbles are highest. The kinetic limit is calculated from a pressure difference in an isothermal process between the meta stable state and saturated state. The production rate of critical bubbles increases rapidly over a short range of pressure differences where the maximum change in production rate is set as the kinetic limit. The thermodynamic spinodal is defined as eq. 16.

$$\left(\frac{\partial p}{\partial \rho}\right)_T = 0, \tag{16}$$

During the isentropic expansion, the liquid is metastable before it undergoes a phase transition to a two-phase mixture of gas and liquid. The calculated states are presented in table 2. The pressures behind the evaporation wave for both initial pressures are still higher than atmospheric pressure, and the expansion across the evaporation wave is significant due to the velocities of the wave.

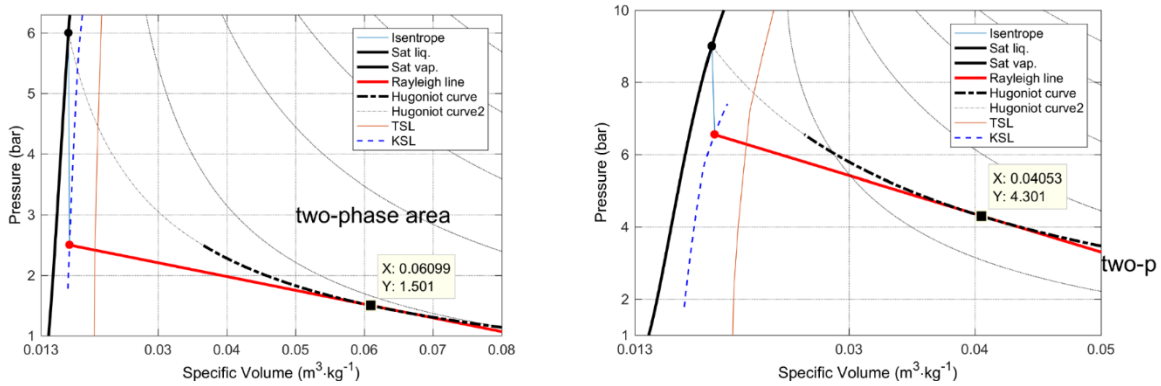

Figure 6: The expansion and following phase transition process in LH2-BLEVE for 6 bara (Left) and 9 bara (Right) initial saturation state. The Rayleigh line is tangent to the Hugoniot curve, where the connected state is the CJ state.

Table 2. Calculated velocities and state data for initial pressure at 12, 9 and 6 bara saturated LH_2.

Calculated state variables	State	Symbol	Unit	Scenario1	Scenario 2	Scenario 3
Temperature	0	T_0	K	32.6	30.7	28.3
Pressure	0	P_0	bar	12	9.0	6.0
	1	P_1	bar	9.8^{TSL}	6.55^{KSL}	2.5^{KSL}
	2	P_2	bar	6.8	4.3	1.5
Velocity	1	u_1	ms^{-1}	104.4	62.8	25.9
Density	0	ρ_0	kgm^{-3}	42.95	52.36	58.82
	1	ρ_1	kgm^{-3}	41.84	51.79	58.14
	2	ρ_2	kgm^{-3}	25.32	24.67	16.40

3.1 Results CFD

For analysis of the CFD results from the two-fluid equations, the time and length scales are made non-dimensional. Characteristic length is the radius of the liquid state in the domain, eq. 17 and characteristic velocity is the speed of sound in the initial liquid state. This leads to a characteristic time equal to the time for the first rarefaction wave to propagate from the liquid interphase to the center of the domain, eq. 18.

$$L = \frac{R}{R_{LH_2}}, \tag{17}$$

$$T = \frac{tc}{R}, \tag{18}$$

Figure 7. shows the initial expansion and phase transition in pressure and liquid volume fraction. The evaporation front propagating into the metastable liquid is still close to non-dimensional distance 1. The pressure drops rapidly behind the phase transition front, making it difficult to determine the actual state behind the front. The pressure is close to 3 bara behind the rapid drop in liquid volume fraction. The density, shown in Fig. 8, changes slightly over the liquid, expanding from a saturated state to a metastable state. Since the gas phase expands due to the lower pressure in the metastable state, the liquid volume fraction is also reduced. The density behind the rapid drop in volume fraction is about 22 kg/m^3.

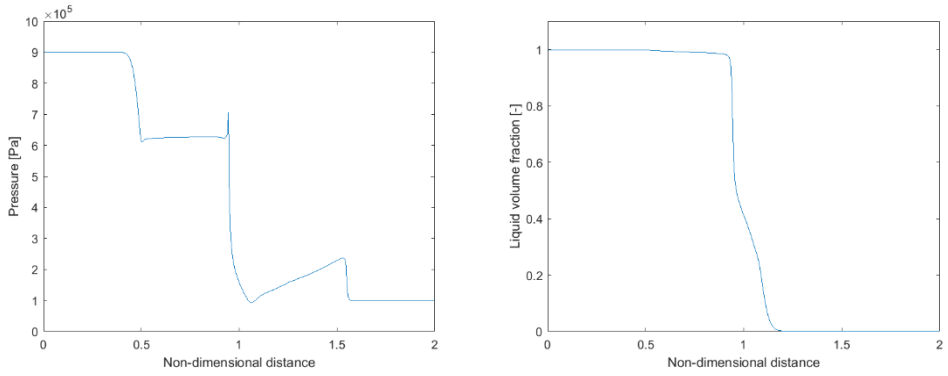

Figure 7: Pressure (Left) and liquid volume fraction (Right) vs. non-dimensional distance at T = 0.74, initial state is 9 bara saturated liquid.

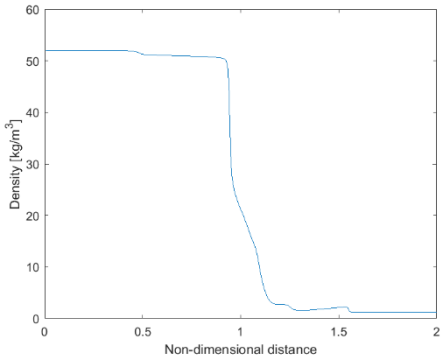

Figure 8: Density vs. non-dimensional distance at T = 0.74 initial state is 9 bara saturated liquid.

Figure 9 shows a wave diagram from the pressure contours in a distance-time diagram. At time zero, the leading shock wave propagates into the air towards the right. The rarefaction wave propagates into the liquid towards the left followed by the phase transition front. The reflected rarefaction wave reaches the phase transition front at about time = 5, leading to a faster phase transition rate. The spherical expansion causes an over-expansion that leads to heavy two-phase mixture flowing towards and focusing in the center of the domain. The higher overpressure causes a secondary shock wave propagating behind the leading shock. The speed of the evaporation wave, before the reflected rarefaction wave reaches the evaporation front, is about 0.1. The dimensionless velocity is a Mach-number, since the characteristic velocity is the sound speed in the liquid hydrogen. The modelled sound speed is about 750 m/s from the stiffened gas EOS, leading to an evaporation front speed of 75 m/s. The first and secondary shocks are shown in Fig. 10 (Left). The maximum blast overpressure as a function of distance is shown in Fig. 10 (Right).

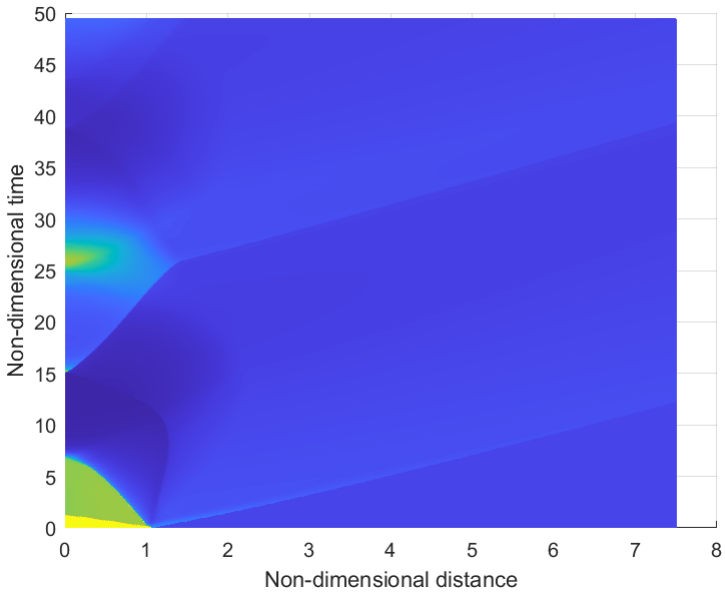

Figure 9: Pressure contours in a distance-time diagram, initial state is 9 bara saturated liquid.

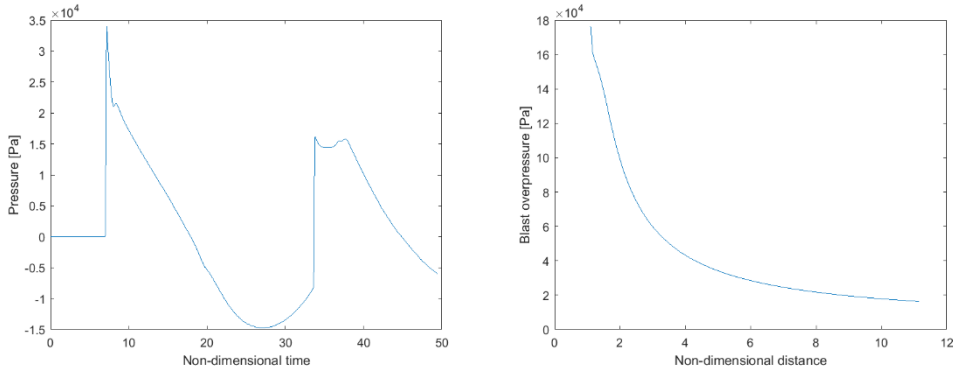

Figure 10: Left: Simulated pressure vs. time at non-dimensional distance 5. Right: Simulated blast overpressure vs. non-dimensional distance, initial state is 9 bara saturated liquid.

4.0 DISCUSSION

The models that form the CFD-method are based on linear equations of state. This simplification is done to be able to use a shock-capturing method for the hyperbolic part of the conservation equations. The liquid phase is modelled as a stiff gas with two model parameters for the liquid state (e.g. γ_1 and p_∞). These two parameters are dependent on the liquid state, and the values used in the present work is fitted to real gas speed of sound and isentrope from the initial state of 9 bara. A third model parameter for the thermodynamic states is the e* that sets the difference in internal energy for the two phases to the energy of vaporization. The liquid thermodynamic state after the phase transition will most likely not be produced correctly by the same parameters as for the pre-expansion liquid state. Nevertheless, it seems like the present simple approach can qualitatively describe the complex thermodynamic processes occurring during a BLEVE event. Results from the CFD simulations are similar to the Rankine Hugoniot calculations. The pressure after the initial phase transition process is lower in the CFD simulations than for the RH calculations, and the simulated evaporation front speed is a bit higher. The expansion of the post phase transition front state quickly reduces the pressure and changes the phase composition towards higher gas volume fraction. This rapid pressure drop is due to the spherical expansion. The propagating leading shock wave propagating into the surrounding air (Fig. 10) shows significant overpressure of 20 kPa at 10 liquid volume radii distance. The blast overpressure decay is also slow since the positive phase of the overpressure is comparatively long. This long positive phase duration will lead to high impulses even at lower overpressures. The ejected two-phase mixture has a high density, and a stagnation of the products will produce larger loads on possible surroundings. The contact surface will not travel far from the initial liquid source due to over-expansion, but people and obstructions close by could be severely affected.

5.0 CONCLUSION

The Rankine Hugoniot analysis presented for LH_2 is based on a similar analysis performed for CO_2 where the results were compared with experimental data. Since there are no experimental data on LH_2-BLEVEs, the present results are not validated, but there is some confidence in the results due to the extension from the work on CO_2. The present methods can be seen as suggestions to further research activities leading to further experimental validation. The analysis shows that the expansion of fluid due to phase transition can sustain a shock wave propagating into the surrounding air. The blast wave decays slowly due to long positive phase in the blast pressure.

If the initial state of the hydrogen is super critical, which can be possible during heating of a LH_2 tank, the expansion and BLEVE process might be different than what is proposed here. Some theoretical work [18] has been done on very high initial pressures that shows a stronger blast wave than presented in the present work.

References

1. Hansen, P. M., Gaathaug, A. V., Bjerketvedt, D. and Vaagsaether, K. 'The behavior of pressurized liquefied CO2 in a vertical tube after venting through the top', *International Journal of Heat and Mass Transfer*, **108, Part B**, 2017, pp. 2011-2020.
2. Hansen, P. M., Gaathaug, A. V., Bjerketvedt, D. and Vaagsaether, K. ' Rapid depressurization and phase transition of CO2 in vertical ducts – Small-scale experiments and Rankine-Hugoniot analyses, *Journal of Hazardous Materials*, **365,** 2019, pp. 16-25.
3. Mjaavatten, A. H2 and CO2 thermodynamics. *https://www.github.com/are-mj/thermodynamics*
4. Span, R. and Wagner, W. A new equation of state for carbon dioxide. *Journal of Physical and Chemical Reference Data*, **25**, 1996, pp. 1509-1596.
5. Blander, M. and Katz, J. L. Bubble nucleation in liquids. *AlChE Journal*, **21(5),** 1975, pp. 833-848.
6. Chaves, H. ´Phasenübergänge und wellen bei der entspannung von fluiden hoher spezifischer wärme´ *PhD thesis, Georg-August-Universität*, 1984, Göttingen
7. Thompson, P. A., Chaves, H., Meier, G. E. A., Kim, Y. G. and Speckmann, H. D. 'Wave splitting in a fluid of large heat capacity', *Journal of Fluid Mechanics*, **185**, 1987, pp. 385-414.
8. J.E. Shepherd, S, McCahan, J Cho, Evaporation Wave Model for Superheated Liquids, *In G. E. A. Meier & P. A.Thompson (Eds.), Adiabatic Waves in Liquid-Vapor Systems: IUTAM Symposium Göttingen*, 1989, Berlin, Heidelberg: Springer Berlin Heidelberg, pp. 3-12.
9. Hill, L. G. An experimental study of evaporation waves in a superheated liquid. *PhD thesis, California Institute of Technology*, 1991, Pasadena, California.
10. Frost, D. L., Lee, J. H. S. and Ciccarelli, G. 'The use of Hugoniot analysis for the propagation of vapor explosion waves', *Shock Waves*, **1(2)**, 1991, pp. 99-110.
11. Simões–Moreira, J. R. and Shepherd, J. E. 'Evaporation waves in superheated dodecane', *Journal of Fluid Mechanics*, **382**, 1999, pp. 63-86.
12. Reinke, P. ´Surface Boiling of Superheated Liquid´, *PhD thesis, Energy Technique Institute*, 1997, Zürich.
13. Reinke, P. and Yadigaroglu, G. 'Explosive vaporization of superheated liquids by boiling fronts', *International Journal of Multiphase Flow*, **27(9)**, 2001, pp. 1487-1516.
14. Simões-Moreira, J. R. ´Adiabatic evaporation waves´, *PhD thesis, Rensselaer Polytechnic Institute*, 1994, Troy, New York.
15. Simões-Moreira, J. R. 'Oblique evaporation waves', *Shock Waves*, **10(4),** 2000, pp. 229-234.
16. Angelo, E., Simões Moreira, J. R. and Barrios, D. B. 'Theory and occurrence of evaporation waves', *Proceedings of COBEM 2005, 18th International Congress of Mechanical Engineering*, 2005, Ouro Preto, MG.
17. Stutz, B. and Simões-Moreira, J. R. 'Onset of boiling and propagating mechanisms in a highly superheated liquid - the role of evaporation waves', *International Journal of Heat and Mass Transfer*, **56(1–2),** 2013 pp. 683-693.
18. Nayak, S., Garcia, S., Carreto, V., Mannan, M.S. 'Can a liquid hydrogen storage tank BLEVE?', AiChE Annual Meeting, October 17. 2011. https://www.aiche.org/academy/videos/conference-presentations/can-liquid-hydrogen-storage-tank-bleve